Er^{3+} ion concentration effect on transient and steady-state behavior in Er^{3+}:YAG crystal

Asadpour Seyyed Hossein† and Rahimpour Soleimani H

Department of Physics, University of Guilan, Rasht, Iran

(Received 1 March 2014; revised manuscript received 13 April 2014; published online 20 August 2014)

The effect of Er^{3+} ion concentration on transient and steady-state behavior in 45-nm Er^{3+}:YAG crystal is investigated. It is shown that by changing the signal field, the coherent field and the concentration of Er^{3+} ions in the crystal, the absorption, dispersion, and group index of the weak probe field can be adjusted. Also, it is found that the probe absorption occurs in the presence of population inversion and probe amplification is obtained in the absence of population inversion.

Keywords: Er^{3+} ion concentration, absorption, dispersion, group index

PACS: 42.65.Pc, 68.65.Fg **DOI:** 10.1088/1674-1056/23/10/104223

1. Introduction

It is well known that quantum coherence and interference can lead to many interesting phenomena in nonlinear and quantum optics. Electromagnetically induced transparency (EIT),[1,2] lasing without inversion (LWI),[3–5] four-wave mixing (FWM),[6–10] large refractive index,[10–14] electron localization,[15–19] optical bistabilty (OB) and multistability (OM),[20–29] and many other interesting phenomena[30–39] have been studied theoretically and experimentally by many research groups in recent years. More recently, it has been shown that semiconductor quantum wells (SQWs) and quantum dots (SQDs) have properties similar to atomic systems such as discrete energy levels and have many essential advantages that the atomic media do not have, such as long dephasing times and large electric dipole moments due to their small effective electron mass. Therefore, many kinds of nonlinear quantum optical phenomena such as EIT,[40–42] OB and OM,[43–55] Kerr nonlinearity,[56,57] and other phenomena[58–60] based on the quantum coherence and interference in SQWs and SQDs have also been investigated recently.

Also recently, in an optically dense rare-earth solid crystal, EIT has been analyzed.[61] EIT in solid crystals has potential applications in lasing without inversion,[62] enhanced FWM,[63] Kerr nonlinearity,[64] OB and OM,[54,65] and enhancing the refractive index.[14] Yttrium aluminum garnet (YAG) is an excellent optical host material compared with others. And Er^{+3}-doped YAG crystal is an efficient active medium for lasers operating in the middle infrared band, coinciding with the telecommunications band. However, most experiments and theoretical investigations in solid crystals have been executed under the same doping concentration of ions. But, in Ref. [66], Xu *et al.* reported their study of the effect of Er^{3+} concentration on electromagnetically induced transparency in two types of three-level schemes. In rare-earth-doped crystals, both the decay rate of population and the electric dipole moment vary as a function of phonon decay and the interaction among ions.[67]

Therefore, in this paper we examine the effect of the concentration of doped ion on the transient and steady state behaviors of absorption and dispersion, and on group index and electron population in four-level Er^{3+}:YAG crystal. Furthermore, our study is much more useful than the similar study of gases, due to our flexible design and the widely modifiable parameters. Therefore, our schemes are very suitable for building greater understanding experimentally.

2. Model and equations

Figure 1 shows a four-level Er^{3+} ionic system in 45-nm Er^{3+}-doped YAG crystal. The energy-level scheme is relevant to the Er^{3+} ions in Er^{3+}:YAG crystal, where levels $|1\rangle$, $|2\rangle$, $|3\rangle$, and $|4\rangle$ correspond to Er^{3+} ion energy levels $^4I_{15/2}$, $^4I_{13/2}$, $^4I_{9/2}$, and $^4S_{3/2}$ respectively. The details of the level structure and the corresponding transition wavelength can be found in Ref. [68]. In this scheme, a strong coupling field with Rabi-frequency Ω_c drives the $|3\rangle \leftrightarrow |4\rangle$ transition. A weak probe field with Rabi-frequency Ω_p couples the $|2\rangle \rightarrow |3\rangle$ transition. While the signal field with Rabi-frequency Ω_s drives the transition $|1\rangle \rightarrow |3\rangle$. In the interaction picture, the semi-classical interaction Hamiltonian H_I of this system under the dipole and rotating wave approximation can be represented as:

$$H_I = \hbar \begin{pmatrix} 0 & 0 & -\Omega_s & 0 \\ 0 & \Delta_s - \Delta_p & -\Omega_p & 0 \\ -\Omega_s & -\Omega_p & \Delta_s & -\Omega_c \\ 0 & 0 & -\Omega_c & \Delta_c + \Delta_s \end{pmatrix}, \quad (1)$$

where the frequency detunings of these three optical fields are defined as $\Delta_c = \omega_c - \omega_{34}$, $\Delta_p = \omega_p - \omega_{23}$, and $\Delta_s = \omega_s - \omega_{13}$ respectively.

†Corresponding author. E-mail: s.hosein.asadpour@gmail.com

© 2014 Chinese Physical Society and IOP Publishing Ltd

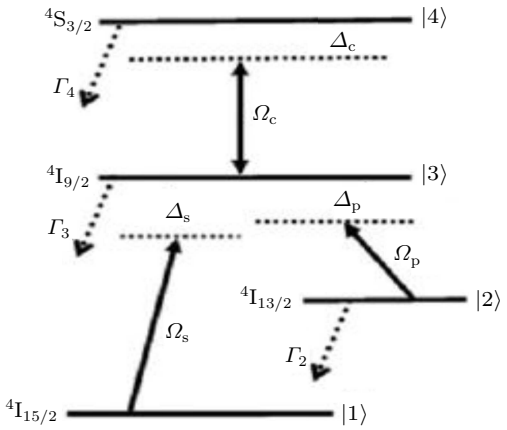


Fig. 1. The Er^{3+}:YAG crystal interacts with three laser fields. Probe field couples $|2\rangle \leftrightarrow |3\rangle$ transition, control field drives $|3\rangle \leftrightarrow |4\rangle$ transition, and signal field is acting on $|1\rangle \leftrightarrow |3\rangle$ transition.

With the usual phenomenological addition of relaxation processes Λ_ρ, the master equation of motion for the density operator in the system in the interaction picture can be written as:

$$\frac{\partial \rho}{\partial t} = -\mathrm{i}[H_\mathrm{I}, \rho] + \Lambda_\rho. \tag{2}$$

By expanding Eq. (2), the density matrix equations of motion for this system can be obtained:

$$\begin{aligned}
\dot{\rho}_{11} &= \Gamma_{21}\rho_{22} + \Gamma_{31}\rho_{33} + \Gamma_{41}\rho_{44} - \mathrm{i}\Omega_\mathrm{s}(\rho_{13} - \rho_{31}),\\
\dot{\rho}_{22} &= -\Gamma_{21}\rho_{22} + \Gamma_{32}\rho_{33} + \Gamma_{42}\rho_{44} - \mathrm{i}\Omega_\mathrm{p}(\rho_{23} - \rho_{32}),\\
\dot{\rho}_{33} &= -(\Gamma_{31} + \Gamma_{32})\rho_{33} + \Gamma_{43}\rho_{44} + \mathrm{i}\Omega_\mathrm{s}(\rho_{13} - \rho_{31})\\
&\quad + \mathrm{i}\Omega_\mathrm{p}(\rho_{23} - \rho_{32}) - \mathrm{i}\Omega_\mathrm{c}(\rho_{34} - \rho_{43}),\\
\dot{\rho}_{21} &= -[\gamma_{21} + \mathrm{i}(\Delta_\mathrm{s} - \Delta_\mathrm{p})]\rho_{21} + \mathrm{i}\Omega_\mathrm{p}\rho_{31} - \mathrm{i}\Omega_\mathrm{s}\rho_{23},\\
\dot{\rho}_{31} &= -(\gamma_{31} + \mathrm{i}\Delta_\mathrm{s})\rho_{31} + \mathrm{i}\Omega_\mathrm{s}(\rho_{11} - \rho_{33}) + \mathrm{i}\Omega_\mathrm{p}\rho_{21} + \mathrm{i}\Omega_\mathrm{c}\rho_{41},\\
\dot{\rho}_{41} &= -[\gamma_{41} + \mathrm{i}(\Delta_\mathrm{c} + \Delta_\mathrm{s})]\rho_{41} - \mathrm{i}\Omega_\mathrm{s}\rho_{43} + \mathrm{i}\Omega_\mathrm{c}\rho_{31},\\
\dot{\rho}_{32} &= -(\gamma_{32} + \mathrm{i}\Delta_\mathrm{p})\rho_{32} + \mathrm{i}\Omega_\mathrm{p}(\rho_{22} - \rho_{33}) + \mathrm{i}\Omega_\mathrm{s}\rho_{12} + \mathrm{i}\Omega_\mathrm{c}\rho_{42},\\
\dot{\rho}_{42} &= -[\gamma_{42} + \mathrm{i}(\Delta_\mathrm{c} + \Delta_\mathrm{p})]\rho_{42} + \mathrm{i}\Omega_\mathrm{c}\rho_{32} - \mathrm{i}\Omega_\mathrm{p}\rho_{43},\\
\dot{\rho}_{43} &= -(\gamma_{43} + \mathrm{i}\Delta_\mathrm{c})\rho_{43} + \mathrm{i}\Omega_\mathrm{c}(\rho_{33} - \rho_{44}) - \mathrm{i}\Omega_\mathrm{s}\rho_{41} - \mathrm{i}\Omega_\mathrm{p}\rho_{42},\\
\rho_{11} &+ \rho_{22} + \rho_{33} + \rho_{44} = 1,\\
\rho_{ij} &= \rho^*_{ji},
\end{aligned} \tag{3}$$

where Γ_{ij} $(i, j = 1,2,3,4)$ is the spontaneous emission decay rate from level $|i\rangle$ to level $|j\rangle$, ignoring the collision broadening effect, and

$$\gamma_{21} = \Gamma_{21} + \gamma_{21}^\mathrm{dph}/2, \tag{4}$$
$$\gamma_{31} = (\Gamma_{31} + \Gamma_{32} + \gamma_{31}^\mathrm{dph})/2, \tag{5}$$
$$\gamma_{32} = (\Gamma_{31} + \Gamma_{32} + \Gamma_{21} + \gamma_{32}^\mathrm{dph})/2, \tag{6}$$
$$\gamma_{41} = (\Gamma_{41} + \Gamma_{42} + \Gamma_{43} + \gamma_{41}^\mathrm{dph})/2, \tag{7}$$
$$\gamma_{42} = (\Gamma_{41} + \Gamma_{42} + \Gamma_{43} + \Gamma_{21} + \gamma_{42}^\mathrm{dph})/2, \tag{8}$$
$$\gamma_{43} = (\Gamma_{41} + \Gamma_{42} + \Gamma_{43} + \Gamma_{31} + \Gamma_{32} + \gamma_{43}^\mathrm{dph})/2, \tag{9}$$

are the decay rates of the corresponding transitions. Here, γ_{ij}^dph is the dephasing decay rate of the quantum coherence of the $|i\rangle \leftrightarrow |j\rangle$ transition and determined by electron–electron interface roughness and phonon scattering processes. These processes are the dominant contributors to the dephasing decay rate and the major impediment to the observation of coherent effects in solid materials. The set of Eqs. (1) and (3) can be solved numerically to obtain the steady state response of the medium. In fact, the response of the medium to the applied field is determined by the linear susceptibility χ, which is defined as

$$\chi = \frac{2N\mu_{23}}{\varepsilon_0 E_\mathrm{p}}\rho_{32}. \tag{10}$$

The electric dipole moment between Er^{3+} ion levels $|2\rangle$ and $|3\rangle$ is given by:[69,70]

$$\begin{aligned}
\mu_{23}^2 &= e\left|\langle\psi| r \left|\psi'\right\rangle\right|^2\\
&= \frac{2}{(2J+1)}\frac{2}{(2J'+1)}e^2\\
&\quad \times \sum_{\lambda=2,4,6}\Omega_\lambda \left|\left\langle 4f^N(\alpha SL)J\left\|U^\lambda\right\|4f^N(\alpha' S' J')\right\rangle\right|^2,
\end{aligned} \tag{11}$$

where the eigenvector ψ may be expressed as a linear combination of the unperturbed states corresponding to an arbitrary coupling scheme.[70] The variable Ω_λ is the phenomenological intensity parameter, J and J' are the quantum numbers of angular momentum of levels $|2\rangle$, $|3\rangle$ respectively. The factor 2 in Eq. (11) arose from the Kramer degeneracy of the Stark levels of the Er^{3+} ion. The squared reduced matrix elements $\left|\left\langle 4f^N(\alpha SL)J\left\|U^\lambda\right\|4f^N(\alpha' S' J')\right\rangle\right|^2$ can be obtained from Ref. [71] and the spectral intensity parameters can be described by the empirical formula[67]

$$\Omega_\lambda(10^{-20}) = 1.25X^{1/4}\exp[-0.4(X-A)^{2/3}] + B, \tag{12}$$

where X is the concentration of doped ions and A and B are empirical parameters: $A = 1.0$, $B = 0.33$ for Ω_2; $A = 1.1, B = 0.72$ for Ω_4; and $A = 1.4$, $B = 0.59$ for Ω_6. From Eqs. (11) and (12), it can be seen that the concentration of doped ions greatly affects Ω_λ; moreover it produces a dramatic influence on μ_{ij}.[67] Based on the experimental results,[67] the spectral intensity parameters for the five Er^{3+}:YAG crystals containing Er^{3+} ion concentrations of 29.06, 20.57, 17.38, 0.79, and 0.52 at.% have been calculated and listed in Table 1.

Table 1. Spectral intensity parameters of Er^{3+}:YAG crystals containing different concentrations of Er^{3+} ions at room temperature.[67]

Concentration of Er^{3+} ion crystal/at.%	Spectral intensity parameters/10^{-20} cm^2		
	Ω_2	Ω_4	Ω_6
0.52	1.16	1.52	1.33
0.79	1.35	1.70	1.47
17.38	0.52	0.92	0.79
20.57	0.47	0.87	0.74
29.06	0.40	0.79	0.66

Also the population spontaneous emission probability Γ_{ij} of the Er^{3+}:YAG crystals and electrical dipole moments under different concentrations are listed in Table 2.[67]

Table 2. Radiative transition probabilities and electric dipole momentum of Er^{3+}:YAG crystals with different concentrations of Er^{3+} ions.[67]

Concentration of Er^{3+} ion crystal/at.%	Transition probabilities/s^{-1}						Electric dipole moments/10^{-32} cm
	Γ_{21}	Γ_{31}	Γ_{32}	Γ_{41}	Γ_{42}	Γ_{43}	μ_{23}
0.52	239.1	206.5	68.3	1727.7	676.6	80.7	2.662
0.79	258.8	211.0	76.6	1952.2	767.5	90.0	2.799
17.38	184.6	127.4	46.7	1181.9	462.9	53.6	2.052
20.57	187.8	152.4	48.0	1212.2	474.8	57.5	1.986
29.06	175.4	85.0	44.6	1132.7	442.8	46.7	1.876

Here, we can estimate the dephasing decay rate as $\gamma_{ij}^{\mathrm{dph}} = 15\Gamma_{21}$ according to Refs. [67] and [72].

3. Result and discussion

The numerical results for the steady state and transient behavior with different corresponding parameters are given in (Figs. 2–8). The transient behavior of the probe absorption (a), dispersion (b), and electron population (c) in different levels for 0.52% Er^{3+} ion concentration is shown in Fig. 2. It is assumed that the system is initially at the level $|1\rangle$, so $\rho_{11}(0) = 1$, $\rho_{ij}(0) = 0$ $(i, j = 1, 2, 3, 4)$. At time $t = 0$, the absorption is zero, and once the time increases, the absorption oscillates and finally reaches the steady state value (Fig. 2(a)). The dispersion properties of the probe field are also shown in Fig. 2(b). The investigation of the dispersion is important due to its application in controlling the group velocity of the light pulse from subluminal to superluminal. It can be seen that the positive dispersion increases from zero and reaches the steady state values as time increases. The time evolution of populations in the Er^{3+}:YAG crystal is presented in part (c) of Fig. 2. It can be seen that the maximum value is reached for electron population transfer from level $|3\rangle$ to level $|1\rangle$. However, the steady-state value of electron population in level $|3\rangle$ is greater than that in level $|2\rangle$. Therefore population inversion occurs between levels $|3\rangle$ and $|2\rangle$. The transient behavior of the absorption (a), dispersion (b), and electron population (c) for the large value of the coupling field and a fixed Er^{3+} ion concentration is illustrated in Fig. 3. It can be seen from Fig. 3(a) that the probe laser exhibits periodic amplification and as time passes it reaches to its steady-state value. The dispersion also has oscillatory behavior, but it still has a positive steady-state value (Fig. 3(b)). Thus subluminal light propagation corresponds to probe amplification in the medium. The time evolution of populations in the Er^{3+}:YAG crystal is presented in part (c) of Fig. 3. It can be seen that the electron population in level $|2\rangle$ is enhanced, and simultaneously, it decreases in level $|3\rangle$. Compared with Fig. 2(c), most electron populations transfer to level $|2\rangle$, which cancels the population inversion between levels $|3\rangle$ and $|2\rangle$. Therefore, the probe amplification is obtained in the absence of population inversion which suggests LWI. The steady-state behavior of the above results is displayed in Fig. 4. From Fig. 4(a) we can see that for different values of Rabi frequencies the absorption behavior differs. For $\Omega_c = \Omega_s = 5$, the probe absorption has a peak (solid line), and for $\Omega_c = \Omega_s = 10$, the probe absorption converts into probe gain. The steady-state of probe dispersion and group index is also shown in parts (b) and (c) of Fig. 4. It is found that the slope of dispersion can be changed by altering the Rabi frequencies of applied fields. In this case, slope of dispersion is always positive and weak probe light corresponds to subluminal light propagation. These results agree well with previously published results. The transient behavior of absorption (a), dispersion (b), and electron population (c) for Er^{3+} ion concentration 29.06%, while other controllable parameters are fixed, is displayed in Fig. 5. It can be seen that the probe absorption becomes negative as the Er^{3+} concentration changes from 0.52% to 29.06%. This is to say that the probe absorption changes to probe gain by enhancing the concentration of Er^{3+} ions. However, the behavior of probe dispersion is same as in Fig. 2(b), while the electron populations in different levels contrast with those in Fig. 2(c). It can be seen clearly that the electron population is greater in level $|2\rangle$ than in level $|3\rangle$. Therefore, changing Er^{3+} ion concentration changes the behavior of electron population in Er^{3+}:YAG crystal levels. Thus, the population inversion between levels $|3\rangle$ and $|2\rangle$ cannot happen, and probe gain is obtained in the absence of population inversion which suggests LWI. Thus, Er^{3+} ion concentration along with the Rabi-frequency of the applied field has an essential role in controlling probe absorption and electron population. The steady-state behavior of the above results is also presented in Fig. 6. It can be seen that the probe absorption (a) is negative and the slope of dispersion is positive. The corresponding group index is also shown in part (c) of Fig. 6. These results show that subluminal light propagation corresponds with probe gain in the medium. The effect of Er^{3+} ion concentration on transient behavior of absorption (a), dispersion (b), and population inversion (c) for $\Omega_s \gg \Omega_c$ is displayed in Fig. 7. In Fig. 7(a), it is found that the modification of Er^{3+} concentration can lead to absorption modification. Here by increasing the Er^{3+} concentration from 0.52% to 29.06%, the absorption of the probe field is reduced. The behavior of probe dispersion is related to Er^{3+} ion concentration. It can be seen clearly that by changing the Er^{3+} concentration from 0.52% to 29.06%, the positive dispersion is converted to negative dispersion. Therefore, the group velocity of the light

pulse switches from subluminal to superluminal. At last the effect of Er^{3+} concentration on transient electron population inversion $\rho_{33} - \rho_{22}$ is depicted in part (c) of Fig. 7. One can see that the transient electron population inversion oscillates rapidly to steady state values and by enhancing the concentration of Er^{3+} ions, the value of population inversion is increased. This means that most electrons are trapped in state $|3\rangle$.

The effect of Er^{3+} ion concentration on the transient behavior of absorption (a), dispersion (b), and population inversion (c) for $\Omega_c \gg \Omega_s$ is displayed in Fig. 8. It is easily seen from Fig. 8(a) that the steady-state value of absorption for the probe field is enhanced for 0.79 at.% Er^{3+} ion concentration. However, by enhancing the Er^{3+}-doped ion concentration from 0.79% to 29.06%, the probe absorption converts to probe amplification. The dispersion behavior is also analyzed and it is found that the steady-state value of dispersion for the probe field is altered by changing the concentration of Er^{3+} ions. However, the steady-state values are always positive for any ion concentration (Fig. 8(b)). At last the effect of Er^{3+} concentration on transient electron population inversion $\rho_{33} - \rho_{22}$ is displayed in part (c) of Fig. 8. By enhancing the concentration of Er^{3+}, the population inversion is reduced and finally reaches a negative value. Thus by changing the values of Er^{3+} concentration from 0.52% to 29.06% the population inversion between levels $|3\rangle$ and $|2\rangle$ is canceled. Thus, the probe amplification occurs in the absence of population inversion. This shows that the Er^{3+} ion concentration plays an essential role in producing gain without population inversion (GWI) in the $\Omega_c \gg \Omega_s$ limit.

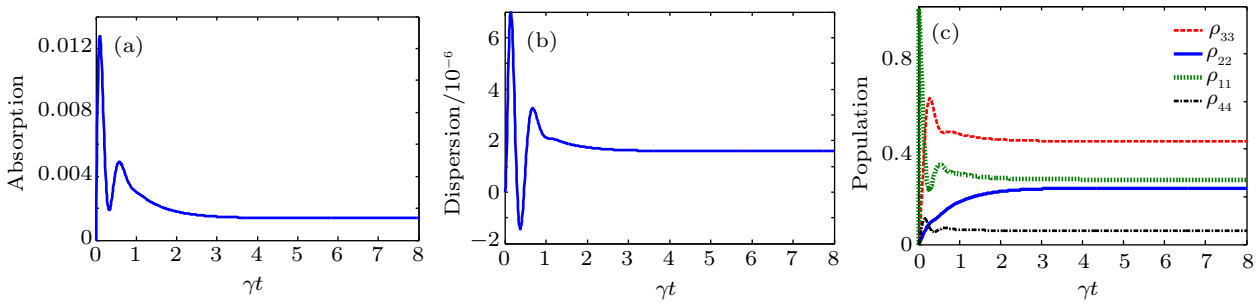


Fig. 2. (color online) Transient behavior of absorption (a), dispersion (b), and electron population (c) in different levels for 0.52% Er^{3+} ion concentration. The selected parameters are $\Omega_c = \Omega_s = 5$, $\Delta_p = \Delta_c = \Delta_s = 0$.

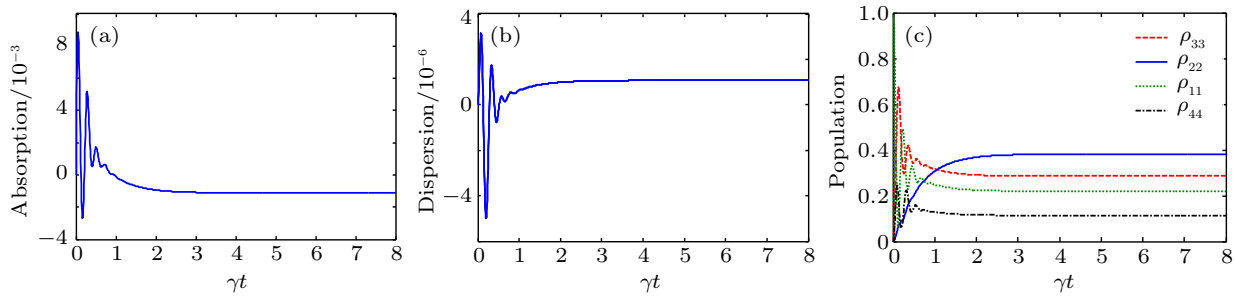


Fig. 3. (color online) Transient behavior of absorption (a), dispersion (b), and electron population (c) in different levels at 0.52% Er^{3+} ion concentration. The selected parameters are $\Omega_c = \Omega_s = 10$, $\Delta_p = \Delta_c = \Delta_s = 0$.

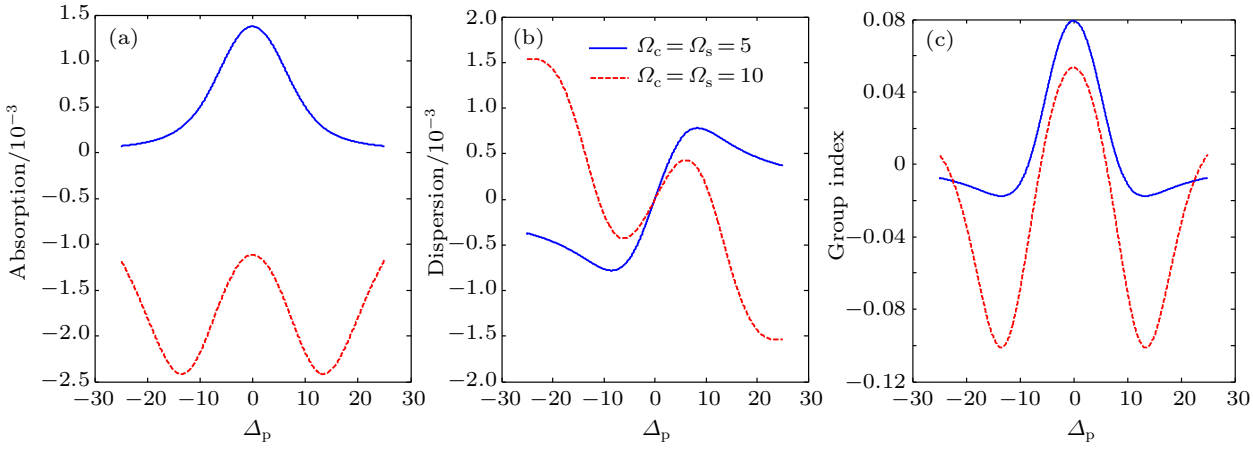


Fig. 4. (color online) Steady-state behavior of absorption (a), dispersion (b), and group index (c) versus probe field detuning at 0.52% Er^{3+} ion concentration. The solid line corresponds to $\Omega_c = \Omega_s = 5$ and dashed line corresponds to $\Omega_c = \Omega_s = 10$. The other selected parameters are same as Fig. 2.

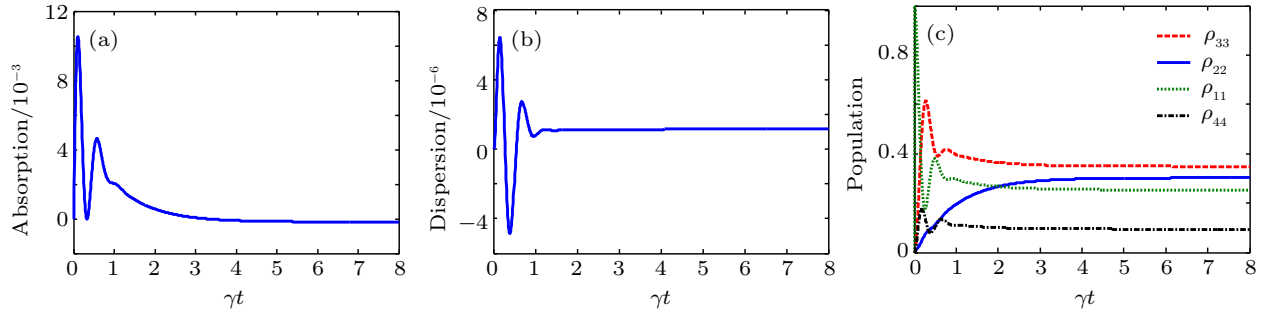


Fig. 5. (color online) Transient behavior of absorption (a), dispersion (b), and electron population (c) in different levels for 29.06% Er^{3+} ion concentration. The selected parameters are same as Fig. 2.

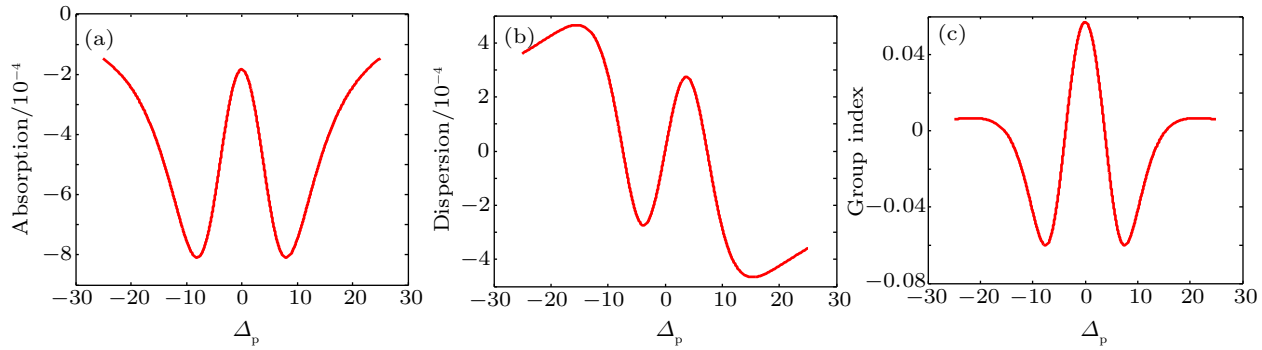


Fig. 6. (color online) Steady-state behavior of absorption (a), dispersion (b), and group index (c) versus probe field detuning at 29.06% Er^{3+} ion concentration. The selected parameters are same as Fig. 5.

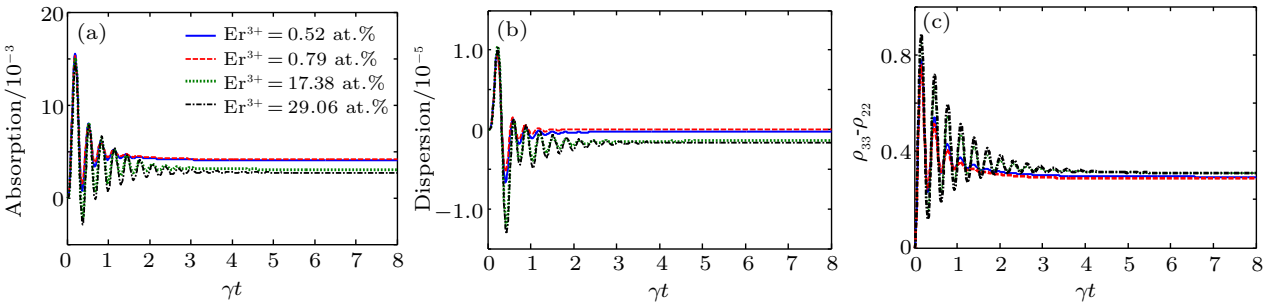


Fig. 7. (color online) Transient behavior of absorption (a), dispersion (b), and population inversion (c) for different values of Er^{3+} ion concentration. The selected parameters are $\Omega_c \ll \Omega_s$, $\Delta_p = \Delta_c = \Delta_s = 0$.

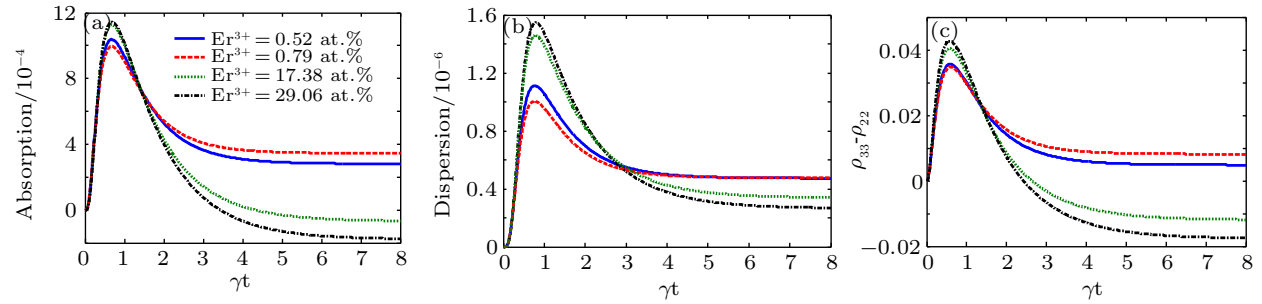


Fig. 8. (color online) Transient behavior of absorption (a), dispersion (b), and population inversion (c) for different values of Er^{3+} ion concentration. The selected parameters are $\Omega_c \gg \Omega_s$, $\Delta_p = \Delta_c = \Delta_s = 0$.

4. Conclusion

In summary, the effect of Er^{3+} ion concentration on transient and steady-state behavior of four-level Er^{3+}:YAG crystal is discussed. It is found that by changing the concentration of Er^{3+}-doped ions in the crystal the probe absorption, dispersion, and electron population can be manipulated. It is found that subluminal and superluminal light propagations, lasing without inversion and absorption with inversion can be obtained by simultaneous adjustment of applied fields and Er^{3+}-ion concentration.

References

[1] Harris S E 1999 *Phys. Today* **50** 36
[2] Wu Y and Yang X 2005 *Phys. Rev. A* **71** 053806
[3] Zhao Y, Huang D and Wu C 1996 *J. Opt. Soc. Am. B* **13** 1614
[4] Zhu Y 1997 *Phys. Rev. A* **55** 4568
[5] Bai Y F, Guo H, Sun H, Han D G, Liu C and Chen X Z 2004 *Phys. Rev. A* **69** 043814
[6] Wu Y and Yang X 2004 *Phys. Rev. A* **70** 053818
[7] Wu Y 2005 *Phys. Rev. A* **71** 053820
[8] Wu Y, Saldana J and Zhu Y 2003 *Phys. Rev. A* **67** 013811
[9] Wu Y, Payne M G, Hagley E W and Deng L 2004 *Phys. Rev. A* **69** 063803
[10] Wu Y, Yang X, Sun C P, Zhou X J and Wang Y Q 2000 *Phys. Rev. A* **61** 043604
[11] Xu H F, Fu A B, Qin L and Jin S W 2013 *Superlattices and Microstructures* **58** 53
[12] Wang Z, Yu B, Zhen S and Wu X 2013 *J. Lumin.* **134** 272
[13] Sadeghi S M, Van Driel H M and Fraser J M 2000 *Phys. Rev. B* **62** 15386
[14] Zhang H F, Wu J H, Su X M and Gao J Y 2002 *Phys. Rev. A* **66** 053816
[15] Sahrai M, Tajalli H, Kapale K T and Zubairy M S 2005 *Phys. Rev. A* **72** 013820
[16] Wang Z 2011 *Opt. Commun.* **284** 262
[17] Wang Z and Yu B 2014 *Laser Phys. Lett.* **11** 035201
[18] Wang Z and Yu B 2012 *Phys. Lett. A* **376** 2264
[19] Li J H, Yu R, Liu M, Ding C and Yang X 2011 *Phys. Lett. A* **375** 3978
[20] Li J H, Lü X Y, Luo J M and Huang Q J 2006 *Phys. Rev. A* **74** 035801
[21] Asadpour S H and Eslami-Majd A 2012 *J. Lumin.* **132** 1477
[22] Osman K I 2006 *Opt. Commun.* **259** 194
[23] Osman K I and Joshi A 2013 *Opt. Commun.* **293** 86
[24] Joshi A and Xiao M 2010 *J. Mod. Opt.* **57** 1196
[25] Li J H 2007 *Physica D* **228** 148
[26] Joshi A, Yang W and Xiao M 2003 *Phys. Rev. A* **68** 018506
[27] Wang Z and Xu M 2009 *Opt. Commun.* **282** 1574
[28] Xiao Z H and Kim K 2010 *Opt. Commun.* **283** 2178
[29] Wu J, Lu X Y and Zheng L 2010 *J. Phys. B: At. Mol. Opt. Phys.* **43** 161003
[30] Wu Y and Yang X 2007 *Phys. Rev. Lett.* **98** 013601
[31] Li J H, Yu R, Hao X, Zheng Z and Yang X 2009 *Opt. Commun.* **282** 4384
[32] Naseri T, Asadpour S H and Sadighi-Bonabi R 2013 *J. Opt. Soc. Am. B* **30** 641
[33] Hamedi H R, Asadpour S H, Sahrai M, Arzhang B and Taherkhani D 2013 *Opt. Quantum Electron.* **45** 295
[34] Wu Y and Deng L 2004 *Phys. Rev. Lett.* **93** 143904
[35] Wu Y and Deng L 2004 *Opt. Lett.* **29** 2064
[36] Yang W X, Chen A X, Lee R K and Wu Y 2011 *Phys. Rev. A* **84** 013835
[37] Hao X Y, Li J H, Liu J B, Song P J and Yang X 2008 *Phys. Lett. A* **372** 2509
[38] Zhang D, Li J H, Ding C and Yang X 2012 *Phys. Lett. A* **376** 1978
[39] Wu Y and Yang X 2007 *Phys. Rev. A* **76** 013832
[40] Zhao Y, Wu C K, Ham B S, Kim M K and Awad E 1997 *Phys. Rev. Lett.* **79** 641
[41] Ichimura K, Yamamoto Y and Gemma N 1998 *Phys. Rev. A* **58** 4116
[42] Nikonov D E, Imamoglu A and Scully M O 1999 *Phys. Rev. B* **59** 12212
[43] Li J H 2007 *Phys. Rev. B* **75** 155329
[44] Li J H 2007 *Opt. Commun.* **274** 366
[45] Joshi A and Xiao M 2004 *Appl. Phys B: Lasers Opt.* **79** 65
[46] Wang Z and Fan H 2010 *J. Lumin.* **130** 2084
[47] Wang Z, Zhen S, Wu X, Zhu J, Cao Z and Yu B 2013 *Opt. Commun.* **304** 7
[48] Wang Z and Yu B 2013 *J. Opt. Soc. Am. B* **30** 2915
[49] Zhang D, Yu R, Li J H, Ding C and Yang X 2013 *Phys. Lett. A* **377** 2621
[50] Li J H, Hao X, Liu J and Yang X 2008 *Phys. Lett. A* **372** 716
[51] Wang Z and Yu B 2013 *J. Appl. Phys.* **113** 113101
[52] Wang Z 2009 *Opt. Commun.* **282** 4745
[53] Wang Z, Yu B, Zhen S, Wu X, Zhu J and Cao Z 2012 *Superlattices and Microstructure* **51** 324
[54] Wang Z 2011 *J. Lumin.* **131** 2404
[55] Asadpour S H, Jaberi M and Rahimpour Soleimani H 2013 *J. Opt. Soc. B* **30** 1815
[56] Asadpour S H, Sahrai M, Sadighi-Bonabi R, Soltani A and Mahrami H 2011 *Physica E* **43** 1759
[57] Asadpour S H, Hamedi H R and Sahrai M 2012 *J. Lumin.* **132** 2188
[58] Imamoglu A and Ram R J 1996 *Opt. Lett.* **131** 333
[59] Lee C R 2004 *Appl. Phys. Lett.* **86** 201112
[60] Frogley M D, Dynes J F, Beck M, Faist J and Philips C 2006 *Nat. Mater.* **5** 175
[61] Ham B S, Hemmer P R and Shahriar S M 1997 *Opt. Commun.* **144** 227
[62] Zibrov A S and Lukin M D 1995 *Phys. Rev. Lett.* **75** 1499
[63] Ham B S, Shahriar S M and Hemmer P R 1997 *Opt. Lett.* **22** 1138
[64] Ghaforyan H, Hamedi H R, Khaledi-Nasab A, Jafarzadeh H, Asadpour S H, Hosseini S M and Sahrai M 2013 *J. Mod. Opt.* **60** 674
[65] Wang Z 2010 *Opt. Commun.* **283** 3291
[66] Xu H, Dai Z and Jiang Z 2002 *Phys. Lett. A* **294** 19
[67] Wang Q Y, Zhang S Y and Jia Y Q 1993 *J. Alloys Compd.* **202** 1
[68] Xu H L and Kroll S 2005 *J. Lumin.* **111** 191
[69] Judd B R 1962 *Phys. Rev.* **127** 750
[70] Ofelt G S 1962 *J. Chem. Phys.* **37** 511
[71] Kaminski A, Mironov V S, Kornienko A, Bagaev S N, Boulon G, Brenier A and Di Bartolo B 1995 *Phys. Status Solidi A* **151** 231
[72] Zhang H F, Dai Z W, Zhang B, Wu J H and Gao J Y 2003 *Chin. Phys.* **12** 964